

# Anti-Hong-Ou-Mandel effect with entangled photons

Anton N. Vetlugin<sup>1\*</sup>, Ruixiang Guo<sup>1</sup>, Cesare Soci<sup>1\*</sup>, and Nikolay I. Zheludev<sup>1,2</sup>

<sup>1</sup>Centre for Disruptive Photonic Technologies, SPMS, TPI, Nanyang Technological University, Singapore 637371

<sup>2</sup>Optoelectronics Research Centre and Centre for Photonic Metamaterials, University of Southampton, Southampton SO17 1BJ, United Kingdom

\*Corresponding author. Email: [a.vetlugin@ntu.edu.sg](mailto:a.vetlugin@ntu.edu.sg) (A.N.V.); [csoci@ntu.edu.sg](mailto:csoci@ntu.edu.sg) (C.S.)

In the classical Hong-Ou-Mandel (HOM) effect pairs of photons with bosonic (fermionic) spatial wavefunction coalesce (anti-coalesce) when mixed on a lossless beamsplitter. Here we report that the presence of dissipation in the beamsplitter allows the observation of the anti-HOM effect, where bosons anti-coalesce and fermions show coalescent-like behavior. We provide an experimental demonstration of the anti-HOM effect for both bosonic and fermionic two-photon entangled states. Beyond its fundamental significance, the anti-HOM effect offers applications in quantum information and metrology where states of entangled photons are dynamically converted.

## I. INTRODUCTION

The Hong-Ou-Mandel (HOM) effect (1) occurs when two indistinguishable particles interfere on a beamsplitter. In such process, the output state depends on the symmetry of the two-particle wavefunction. ‘Bosons coalesce and fermions anti-coalesce’ is a common resume of the HOM effect (Fig. 1a-b). This statement was supported by numerous experiments including experiments with photons (2, 3), plasmons (4, 5), phonons (6), atoms (7, 8), collective atomic excitations (9), electrons (10) and levitons (11). Besides being one of the most striking fundamental phenomena, the HOM effect plays a key role in various applications, from timing measurement (12) and lithography (13) to quantum computation (14-16), boson sampling (16, 17) and communication (18, 19).

The nature of the beamsplitter plays an essential role in the HOM effect. For instance, the ‘degree of boson coalescence’ is determined by the difference between reflectance and transmittance of the beamsplitter (20). It is commonly accepted that the presence of dissipative channels of the beamsplitter hampers the HOM effect, thus losses are usually averted in experiments. However, the presence of dissipation may induce non-trivial effects. For instance, theory predicts that carefully designed lossy beamsplitter may reverse the outcome of the two-boson interference, from coalescence to anti-coalescence (21), Fig. 1c. This prediction was experimentally verified in a plasmonic system (22). Similarly, theory predicts that fermions interfering on a lossy beamsplitter may exhibit coalescent-like behaviour (22), Fig. 1d.

In quantum optics, entangled photons may possess either bosonic or fermionic spatial wavefunctions depending on polarization Bell state (23). Bosonic and fermionic regimes of interference are exploited in quantum information and metrology applications where propagating entangled photons are dynamically converted into different states (24-30). The ability to switch between ‘fermionic’ behaviour of bosons and ‘bosonic’ behaviour of fermions, may therefore enrich these protocols and provide new approaches for quantum light manipulation. Recently, the anti-HOM effect was demonstrated for bosonic wavefunctions of (non-entangled) photon pairs by exploiting a non-unitary grating metasurface as a lossy beamsplitter (31). Nevertheless, lack of entanglement in the system and polarization selectivity of the metasurface make this approach unsuitable for non-unitary processing of fermionic wavefunctions.

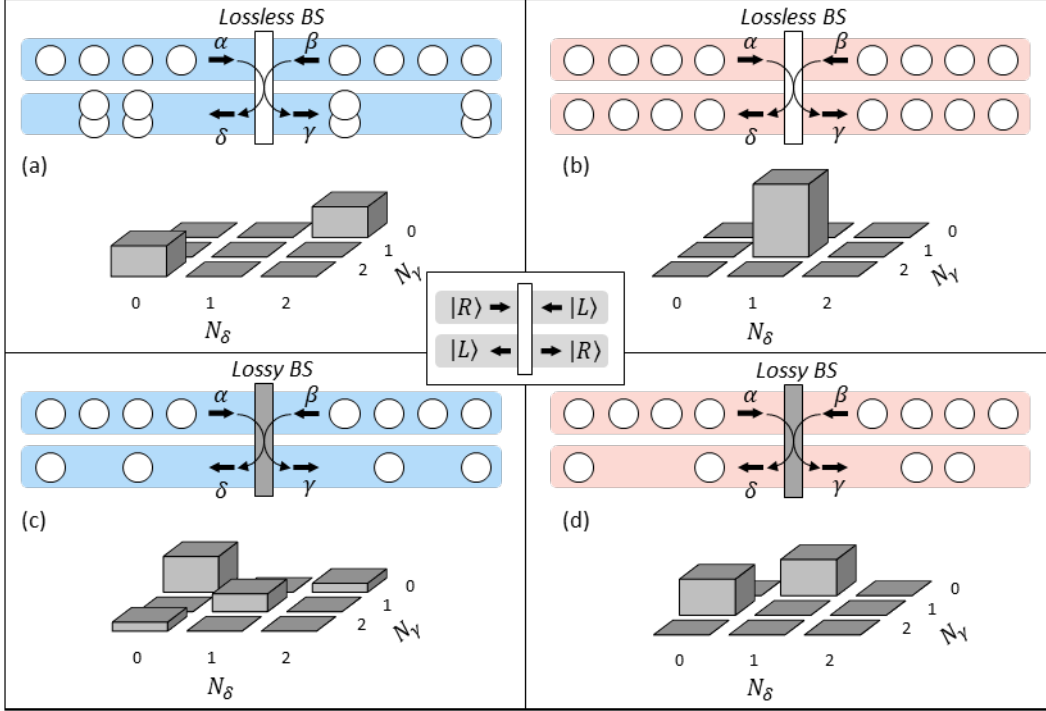


Figure 1. **Hong-Ou-Mandel ((a) and (b)) and anti-Hong-Ou-Mandel ((c) and (d)) effects.** (a) Pairs of bosons enter a lossless beamsplitter through the input ports  $\alpha$  and  $\beta$  and, due to interference, the particles coalesce leaving the beamsplitter through the same output port –  $\gamma$  or  $\delta$ . (b) Pairs of fermions, in contrast, anti-coalesce on a lossless beamsplitter leaving the beamsplitter through different output ports. (c) Boson pairs interfering on the lossy beamsplitter are absorbed with the 50% probability while the rest of the pairs tend to anti-coalescence. (d) Fermion pairs interfering on a lossy beamsplitter experience one particle absorption resulting in coalescent-like behaviour. Particle number distribution ( $N_\gamma$  and  $N_\delta$ ) in output ports of the corresponding beamsplitter is shown for each case. Spatial modes occupied by the particles are defined in the inset in the middle of the figure.

Here, we experimentally study interference of bosonic and fermionic wavefunctions of entangled photons in the absence and presence of dissipation. While bosons (fermions) coalesce (anti-coalesce) as a result of dissipation-free interference, dissipative interference yields the opposite outcome, with bosons (fermions) showing anti-coalescent (coalescent-like) behaviour. To demonstrate this reversed – ‘anti-Hong-Ou-Mandel’ effect, we map the two-photon wavefunction from the original travelling waves (TWs) basis into the basis of the quantized standing waves (QSWs), perform non-unitary transformation in the QSWs basis and, finally, map the wavefunctions back into the original TWs basis (32). The non-unitary transformation of the QSWs is implemented by a subwavelength absorber designed to be sensitive to the symmetry of the QSWs. QSWs based approach is polarization insensitive thus allowing to perform non-unitary transformation of any two-photon states. This opens access to processing of entangled photon states including states with fermionic symmetry which has not been demonstrated before.

We argue that, along with other dissipation-induced phenomena like entanglement generation by dissipation (33, 34) and coherent perfect absorption (35-37) of quantum light (38-46), the anti-HOM effect has a great fundamental and practical importance in quantum optics.

## II. HONG-OU-MANDEL AND ANTI-HONG-OU-MANDEL EFFECTS

Let us consider two indistinguishable photons in the counter propagating geometry, Fig. 1, where the photon wave packets are assumed to be long enough compared to the central wavelength  $\lambda$ . Photons are bosons which put restriction on the symmetry of the *total* wavefunction under the particles permutation. The total wavefunction,  $|\Psi_{\text{pol}}\rangle \otimes |\Psi_{\text{sp}}\rangle$ , contains polarization  $|\Psi_{\text{pol}}\rangle$  and spatial  $|\Psi_{\text{sp}}\rangle$  components. For instance, the symmetric polarization Bell state,

$$|\Psi_{\text{pol}}^{(s)}\rangle = \frac{1}{\sqrt{2}}(|H\rangle_1|V\rangle_2 + |V\rangle_1|H\rangle_2), \quad (1)$$

should be accompanied by the symmetric (bosonic) spatial wavefunction,

$$|\Psi_{\text{sp}}^{(b)}\rangle = \frac{1}{\sqrt{2}}(|L\rangle_1|R\rangle_2 + |R\rangle_1|L\rangle_2). \quad (2)$$

On the other hand, the anti-symmetric polarization Bell state,

$$|\Psi_{\text{pol}}^{(a)}\rangle = \frac{1}{\sqrt{2}}(|H\rangle_1|V\rangle_2 - |V\rangle_1|H\rangle_2), \quad (3)$$

should be accompanied by the anti-symmetric (fermionic) spatial wavefunction,

$$|\Psi_{\text{sp}}^{(f)}\rangle = \frac{1}{\sqrt{2}}(|L\rangle_1|R\rangle_2 - |R\rangle_1|L\rangle_2). \quad (4)$$

Here  $|H\rangle$  ( $|V\rangle$ ) defines the horizontal (vertical) polarization and  $|L\rangle$  ( $|R\rangle$ ) defines the left (right) direction of propagation (inset in Fig. 1). The lower index identifies the photon's number. First, we consider the case when the photons enter a *lossless* beamsplitter which is characterized by the amplitude transmission  $t$  and reflection  $r$  coefficients for which we assume (47)

$$t = |t| \text{ and } r = \pm i|r|. \quad (5)$$

The beamsplitter redistributes each particle between two output ports as  $|L\rangle \rightarrow t|L\rangle + r|R\rangle$  and  $|R\rangle \rightarrow r|L\rangle + t|R\rangle$ . Photons with the bosonic wavefunction tend to leave the beamsplitter through the same output port, and they do so always if  $|t| = |r| = 1/\sqrt{2}$ :  $|\Psi_{\text{sp}}^{(b)}\rangle \rightarrow \frac{1}{\sqrt{2}}(|L\rangle_1|L\rangle_2 + |R\rangle_1|R\rangle_2)$ . In this case, the output photon number distribution contains only terms  $N_\gamma = 2/N_\delta = 0$  and  $N_\gamma = 0/N_\delta = 2$  with a lack of  $N_\gamma = 1/N_\delta = 1$  contribution, Fig. 1a ( $N_\gamma$  and  $N_\delta$  are the number of photons presented at the beamsplitter's output ports  $\gamma$  and  $\delta$ , respectively). In contrast, the fermionic wavefunction is 'immune' to any lossless beamsplitter transformation,  $|\Psi_{\text{sp}}^{(f)}\rangle \rightarrow |\Psi_{\text{sp}}^{(f)}\rangle$ , and the particles are always found in different output ports with characteristic 'anti-coalescent' term  $N_\gamma = 1/N_\delta = 1$  in the output distribution, Fig. 1b. This transformation of the bosonic and fermionic wavefunctions by the lossless beamsplitter is known as the Hong-Ou-Mandel (HOM) effect.

Absence of losses in the HOM effect guarantees unitary beamsplitter transformation and defines the phase relation between coefficients  $t$  and  $r$  in equation (5). Accordingly, the amplitude of the 'anti-coalescent' part ( $N_\gamma = 1/N_\delta = 1$ ) of the bosonic wavefunction after the beamsplitter,  $\sim(t^2 + r^2)$ , decreases. To alter the phase relation between  $t$  and  $r$ , the beamsplitter should possess dissipation channels. The most interesting case is when  $t$  and  $r$  are in-phase or out-of-phase, which maximises the amplitude ( $t^2 + r^2$ ), thus completely changing the interference patterns. In the extreme case of a lossy beamsplitter with

$$t = \pm r = 0.5, \quad (6)$$

photon pairs with the bosonic symmetry (3) experience *probabilistic two-photon absorption* with a high probability of 'anti-coalescent'  $N_\gamma = 1/N_\delta = 1$  output (distribution in Fig. 1c). Conversely, photons with the fermionic wavefunction (4) experience *deterministic one-photon absorption* and the 'anti-coalescent' term  $N_\gamma = 1/N_\delta = 1$  vanishes (distribution in Fig. 1d) (32). As a result, dissipation channels of the beamsplitter induce the anti-HOM effect: bosons show anti-coalescent behaviour while fermions show coalescent-like behaviour.

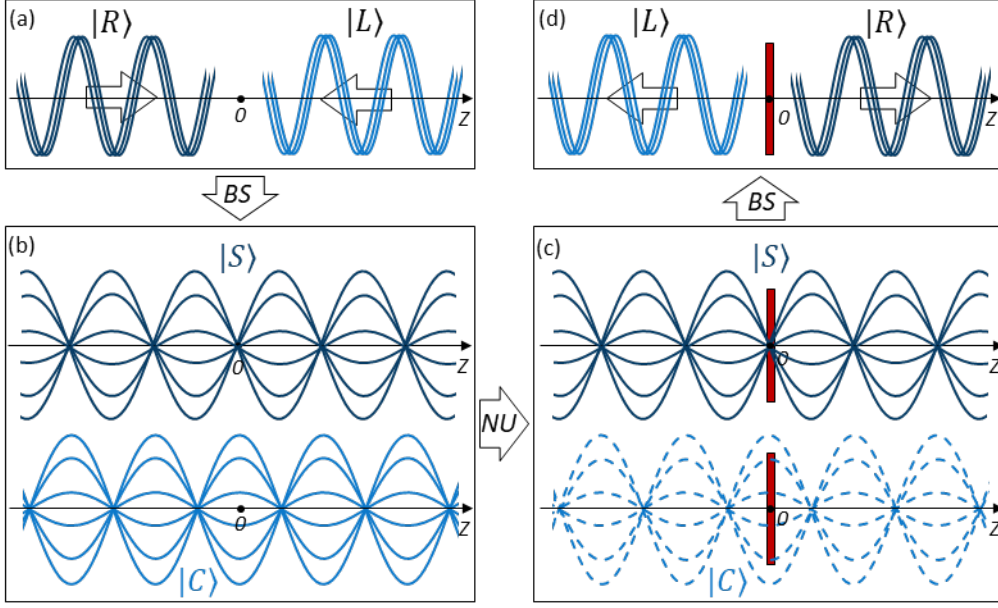


Figure 2. **Anti-HOM effect mediated by non-unitary transformation of quantized standing waves.** From original travelling waves basis (a) we switch to the basis of quantized standing waves (b) by a beamsplitter-like (BS) transformation. The required non-unitary (NU) transformation is achieved by full dissipation of the cosine standing wave by ultrathin absorptive layer, while the sine wave is not affected by this layer (c). The second beamsplitter-like transformation restores the photon state in the original travelling waves basis (d).

To demonstrate the anti-HOM effect for bosonic and fermionic states of entangled photons, the beamsplitter should have equal optical response defined in (6) at both horizontal and vertical polarization of light. To solve the problem of polarization sensitivity of the lossy beamsplitter, the splitting-resonator plasmonic metasurface (40, 41) may be used where polarization-independent operation (42) could be achieved by the meta-molecules design optimization. Here, instead of pursuing the optical response (6), we develop the alternative approach oriented on reconstruction of the output photon distribution shown in Figs. 1c-d. Our approach, based on non-unitary transformation of quantized standing waves (QSWs) (32), allows to achieve the two-photon absorption of bosonic states and the one-photon absorption of fermionic states and, thus, to demonstrate the anti-HOM effect.

Two-photon interference is conventionally treated in the travelling waves (TWs) basis, Fig. 2a. Let us now consider it in the basis of the QSWs, Fig. 2b. Two photon wave packets counter-propagating along the  $z$ -axis,  $\sim \exp(ikz)$  and  $\sim \exp(-ikz)$ , excite two (orthogonal) QSWs with  $\cos(kz)$  and  $\sin(kz)$  spatial distribution ( $k = 2\pi/\lambda$  is the wave number,  $\omega = ck$  is the angular frequency, and  $c$  is the speed of light). The two bases are linked through the beamsplitter-like transformation (32) which allows to express the two-photon state in the new basis:

$$|\Psi_{sp}^{(b)}\rangle \rightarrow \frac{1}{\sqrt{2}}(|S\rangle_1|S\rangle_2 + |C\rangle_1|C\rangle_2), \quad (7)$$

$$|\Psi_{sp}^{(f)}\rangle \rightarrow \frac{1}{\sqrt{2}}(|S\rangle_1|C\rangle_2 - |C\rangle_1|S\rangle_2). \quad (8)$$

Here  $|C\rangle$  ( $|S\rangle$ ) defines the photon occupying the cosine (sine) standing wave. According to (7) and (8), the bosonic particles are always found in the same standing wave, while the fermionic particles are split evenly between the sine and cosine waves (fermionic wavefunction does not change under any beamsplitter transformation). Thus, to perform the ‘bosonic’ *probabilistic two-photon absorption* as

well as the ‘fermionic’ *deterministic one-photon absorption*, one needs to build a dissipative beamsplitter which selectively absorbs one of the QSWs while not affecting the other. This non-unitary transformation can be achieved by ultrathin absorptive layers which are transparent if placed at the nodes of the standing wave, while completely dissipate the standing wave if placed at the anti-nodes. For instance, as shown in Fig. 2c, a single absorptive layer may be placed at the anti-node of the cosine standing wave to achieve absorption of all the excitations of this wave. At the same time, this layer would be located at the node of the sine wave and therefore will not interact with it. After performing this non-unitary transformation, we come back to the original TWs basis by the second beamsplitter-like transformation, Fig. 2d. Here the ‘bosonic’ (two) photons that survive the absorption are split evenly between the  $|L\rangle$  and  $|R\rangle$  outgoing modes, restoring the distribution in Fig. 1c. Similarly, the ‘fermionic’ (one) photon that survives the absorption is split between the propagating modes with distribution shown in Fig. 1d. Remarkably, such lossy beamsplitter constructed in the QSWs basis to selectively absorb standing waves of different symmetry would also have the required optical response,  $t = \pm r = 0.5$ , in the TWs basis, which is necessary to observe the anti-HOM effect. The same result can be achieved, by splitting the absorptive layer into multiple layers and placing them at the anti-nodes of the cosine or sine standing waves.

### III. BOSONIC AND FERMIONIC INTERFERENCE WITH ENTANGLED PHOTONS

To perform the two-particle interference experiment for both bosonic (3) and fermionic (4) wavefunctions in a single platform, we exploit polarization entangled photon pairs. We generate the photons via degenerate type-II spontaneous parametric down conversion (SPDC). Non-linear BBO crystal is pumped by a 405 nm CW laser generating SPDC photon pairs at wavelength of  $\lambda=810$  nm. The photons are counter propagated in the interferometer setup by mirrors (Ms), Fig. 3a. Bell state control is implemented by a set of quarter-half-quarter wave plates placed in one arm of the interferometer. Fast axes of the quarter wave plates are fixed at  $45^\circ$  relative to horizontal axis. Rotation of the half wave plate by  $\varphi/2$  angle around the optical axis induces a phase shift  $\varphi$  between the horizontal and vertical polarization components of the photon (48). Consequently, the two-photon polarization state,  $\frac{1}{\sqrt{2}}(|H\rangle_1|V\rangle_2 + e^{i\varphi}|V\rangle_1|H\rangle_2)$ , can be switched between the symmetric (1),  $\varphi = 0$ , and anti-symmetric (2),  $\varphi = \pi$ , Bell states. We verified preparation of the Bell states through measurement of polarization correlations between the entangled photons by using polarization analysers and single photon avalanche detectors SPAD-1 and SPAD-2 (Excelitas, SPCM-AQRH-14-FC with efficiency of 60% at 810 nm) as shown in circular dashed boxes in Fig. 3a. Coincidence counts are measured as a function of the angle  $\theta_1$  of the analyser placed at the right arm of the interferometer while the angle  $\theta_2$  of the second analyser is fixed at one of the four different values:  $0, \pm\pi/4$  or  $\pi/2$ . As expected, symmetric and anti-symmetric Bell states exhibit identical correlations when measured in horizontal (H) and vertical (V) bases ( $\theta_2 = 0$  and  $\theta_2 = \pi/2$ ) and opposite correlations when measured in diagonal (D) and anti-diagonal (A) bases ( $\theta_2 = \pm\pi/4$ ). The Bell parameter  $S$  for the symmetric (anti-symmetric) Bell state is 2.63 (2.60) where  $S = \sqrt{2}(V_1 + V_2)$  and  $V_1$  ( $V_2$ ) is the visibility of the interference fringes in H/V (D/A) basis (42). The value of  $S$  greater than 2 corresponds to non-classical correlations and the value 2.88 corresponds to the maximally entangled state.

Each photon from the entangled pair passes through a bandpass filter (BPF) with FWHM of 10 nm centered at 810 nm to ensure spectral indistinguishability of the photons. Photonic transverse spatial modes are matched by sending the photons through single mode fibers (not shown in Fig. 3a). Additional half and quarter wave plates in each arm of the interferometer are used to compensate

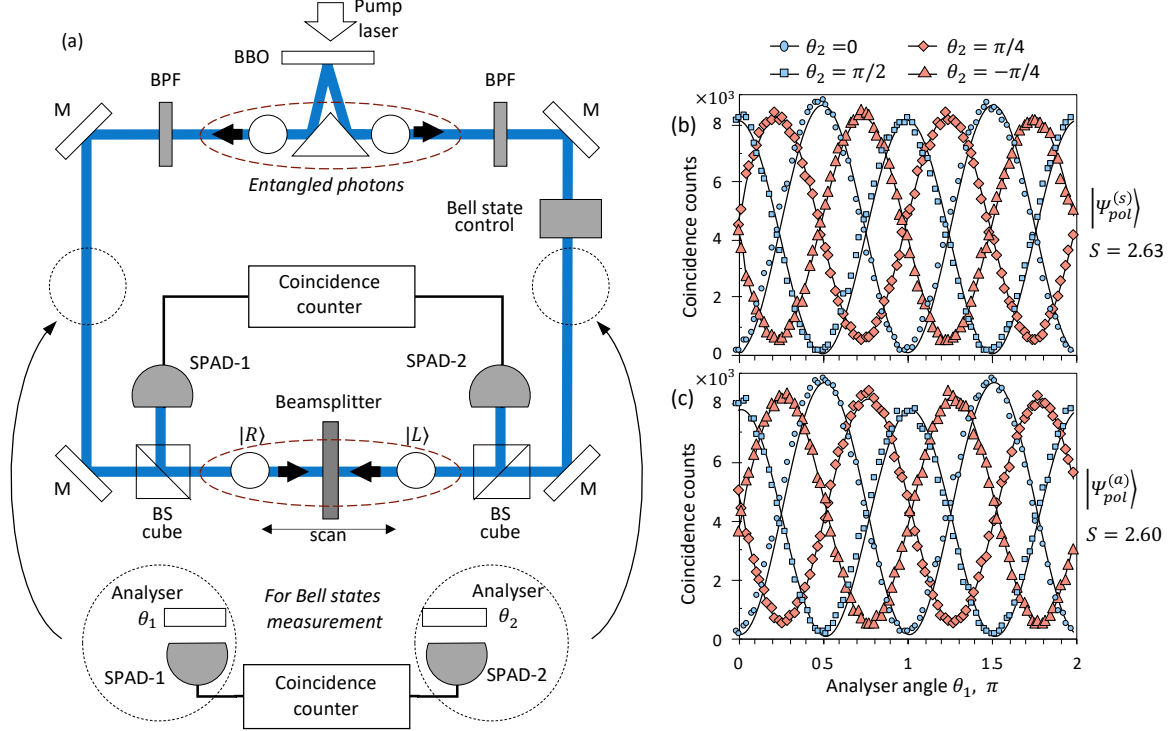


Figure 3. **Bosonic and fermionic interference with entangled photons.** (a) Schematic of the setup for dissipation-free and dissipative two-photon interference with controllable switching between the Bell states. Preparation of the symmetric (b) and anti-symmetric (c) Bell states is verified through measurement of polarization correlations between the entangled photons with apparatus shown in inset in (a). All lines in (b) and (c) are fitting curves.

polarization distortion of the photons passed through the fibers. Finally, indistinguishable photons interfere on the sample – lossless or lossy beamsplitter, placed in the middle of the interferometer. As a lossless beamsplitter, we use a 100 nm thick silicon nitride (SiN) film with reflectance (transmittance) of around 40% (60%) at 810 nm at a normal incidence. As a lossy beamsplitter with  $t \approx +r \approx 1/2$ , we use two 5 nm thick chromium layers deposited on both sides of the SiN film with a thickness  $d = 195$  nm where  $d \approx \lambda/(2n_{SiN})$  and  $n_{SiN} \approx 2.1$  ( $n_{SiN}$  is a refractive index of the SiN film). This structure is designed to place the dissipative metallic layers of a subwavelength thickness at the anti-nodes (nodes) of the sine (cosine) standing wave. Beamsplitter cubes (BS cubes) placed in each arm of the interferometer allow to distinguish between the photons propagating towards and away from the sample. The outgoing photons are detected by SPAD-1 and SPAD-2. By scanning the sample position around the center of the interferometer, we vary the degree of the photons overlap at the sample (time of arrival). In the experiment, we measure coincidence counts (Coincidence counter – IDQ, ID800-TDC with the coincidence window set to 1.62 ns) between the detectors SPAD-1 and SPAD-2 as a function of the sample position.

First, we illuminate the lossless beamsplitter by the bosonic pairs,  $|\Psi_{pol}^{(s)}\rangle \otimes |\Psi_{sp}^{(b)}\rangle$  (blue diamonds in Fig. 4a). When photons arrive at the beamsplitter at different times ('Beamsplitter position'  $\lesssim -30\mu m$  and  $\gtrsim 30\mu m$ ), interference does not happen, and there is a close to 0.5 probability that the particles will take different output ports. These events generate the 'reference' level of the coincidence counts. When the photons overlap at the beamsplitter, the HOM effect occurs: bosons coalesce with the characteristic dip in the coincidence counts measurement. Next, the lossless beamsplitter is illuminated by the fermionic pairs,  $|\Psi_{pol}^{(a)}\rangle \otimes |\Psi_{sp}^{(f)}\rangle$  (red circles in Fig. 4a). In the absence of interference, around half of the particle pairs take the same output port. These events are

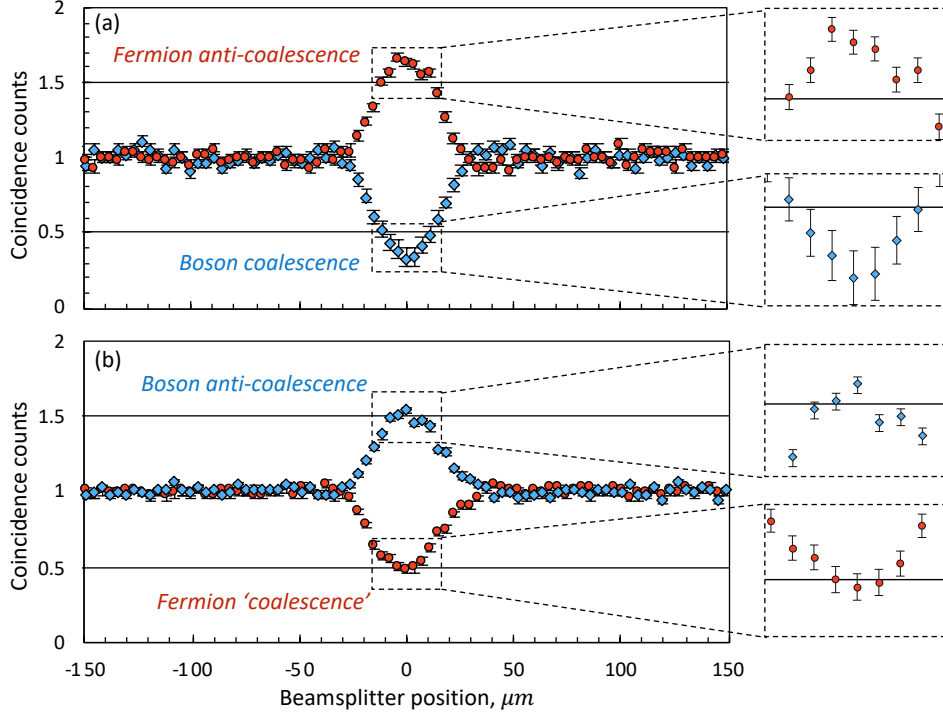


Figure 4. **Hong-Ou-Mandel and anti-Hong-Ou-Mandel experiments.** (a) The HOM experiment: boson coalescence and fermion anti-coalescence are revealed through the dip (blue diamonds) and peak (red circles), respectively, in the coincidence counts measurements. Each point is acquired for 2 seconds and level 1 corresponds to  $\sim 750$  coincidence counts. (b) The anti-HOM experiment: boson anti-coalescence and fermion 'coalescence' are revealed through the peak (blue diamonds) and dip (red circles), respectively, in the coincidence counts measurements. Each point is acquired for 25 seconds and level 1 corresponds to  $\sim 2150$  coincidence counts. Solid black lines show corresponding classical limits. Zoom in in the regions with the lowest and highest coincidence counts are shown on the right-hand side. Error bars are due to the shot noise of the counting.

suppressed when the particles are overlapped at the beamsplitter, and the fermions tend to leave the beamsplitter through different output ports. The number of the coincidence counts rises and the characteristic peak is observed. We note, that the 'bosonic' dip does not reach 0 and the 'fermionic' peak does not reach 2 in Fig. 4a, since the reflectance and transmittance of the beamsplitter are not equal. Also, the deviation of the generated Bell states from the ideal states (1) and (2) impact the visibility since fermionic component adds up to the bosonic state and vice versa.

When the lossless beamsplitter is replaced by the lossy beamsplitter, the result of the coincidence counts measurement changes drastically, Fig. 4b. First, we consider dissipative interference of the bosonic particles,  $|\Psi_{\text{pol}}^{(s)}\rangle \otimes |\Psi_{\text{sp}}^{(b)}\rangle$  (blue diamonds in Fig. 4b). When the photons from the pair arrive at the beamsplitter at different times, there is a 0.5 chance that one of the particles will be absorbed and the survived particle does not contribute to the coincidence counts. The probability of the coincidence count event is  $2 * (0.25 * 0.25) = 0.125$  (both photons are transmitted with the probability of  $0.25 * 0.25$  and both photons are reflected with the same probability). When the photons are overlapped at the beamsplitter, single photon absorption is suppressed, at the same time increasing the probability of the photons to take different output ports (photon number distribution in Fig. 1c). As a result, the peak in the coincidence counts measurement is observed. Next, we illuminate the lossy beamsplitter by the fermionic pairs,  $|\Psi_{\text{pol}}^{(a)}\rangle \otimes |\Psi_{\text{sp}}^{(f)}\rangle$  (red circles in Fig. 4b). For the photons arriving at different times, the probability of the two particles to be detected at different output ports is, again, 0.125. When the fermions are overlapped at the beamsplitter, deterministic

one particle absorption takes place. Since the survived particles does not produce the coincidence counts, the dip in the coincidence counts measurement is detected. We note that the precise tuning of the beamsplitter's parameters and exploitation of the maximally entangled Bell states would allow to reach the maximum possible level of 2 for the 'bosonic' peak and the minimum possible level of 0 for the 'fermionic' dip. We independently checked that the 'bosonic' peak of non-entangled photon pairs (photons were set to the same polarization state) is  $\sim 10\%$  higher than for entangled bosonic pairs. Importantly, all four curves in Fig. 4 cross the corresponding classical limits of 0.5 or 1.5 (22, 49) indicating quantum regimes of interference.

#### IV. SUMMARY AND CONCLUSIONS

We experimentally demonstrated the anti-HOM effect by interfering bosonic and fermionic wavefunctions of entangled photons in the absence and presence of dissipation. We showed that bosons widely accepted as the coalescent particles may display an actual anti-coalescent behaviour (peak in the coincidence counts measurement) if the beamsplitter has dissipation channels. Similar, fermions known as particles with anti-coalescent behaviour may reveal coalescent-like features (dip in the coincidence counts measurement) if they interfere on a lossy beamsplitter. The anti-HOM effect is a fundamental effect relevant to the interference of any two particles in the presence of dissipation, and may be used to substitute the HOM effect in practical applications. Moreover, the ability to switch between fermionic behaviour of bosons and bosonic behaviour of fermions may enrich the quantum information and metrology protocols based on entangled photons with dynamically switchable bosonic and fermionic states.

Beamsplitter-like transformation appears in the interaction between quantum light and matter (50) where light absorption happens due to excitation of inner states of matter. From this point of view, the anti-HOM effect could provide novel approaches for the protocols of quantum memory (51-53), quantum networks and so on. Interference of particles in the presence of light absorption channels may also be extended to other coherent schemes of light illumination including virtual absorption (54), absorption in a coupled matter-cavity systems (55-57) and non-linear regimes of coherent absorption (58). Importantly, demonstrated anti-HOM effect may be considered as a manifestation of the fundamental underlying process – redistribution of particles originally containing in the propagating modes between the quantized standing waves. This picture would allow consideration of coherent phenomena in quantum optics under the new perspective, and interaction protocols based on this mechanism may be realized.

#### Acknowledgement

This work was supported by the Singapore A\*STAR QTE program (SERC A1685b0005), the Singapore Ministry of Education (MOE2016-T3-1-006 (S)), the Singapore NRF-Quantum Engineering Program (NRF-QEP1) and the UK's Engineering and Physical Sciences Research Council (grant EP/M009122/1).

#### References

1. F. Bouchard *et al.*, Two-photon interference: the Hong–Ou–Mandel effect. *Rep. Prog. Phys.* **84**, 012402 (2021).
2. C. K. Hong, Z. Y. Ou, L. Mandel, Measurement of subpicosecond time intervals between two photons by interference. *Phys. Rev. Lett.* **59**, 2044-2046 (1987).
3. J. G. Rarity, P. R. Tapster, Fourth-order interference in parametric downconversion. *J. Opt. Soc. Am. B* **6**, 1221-1226 (1989).
4. R. W. Heeres, L. P. Kouwenhoven, V. Zwiller, Quantum interference in plasmonic circuits. *Nat. Nanotechnol.* **8**, 719-722 (2013).
5. J. S. Fakonas, H. Lee, Y. A. Kelaita, H. A. Atwater, Two-plasmon quantum interference. *Nat. Photonics* **8**, 317-320 (2014).



6. K. Toyoda, R. Hiji, A. Noguchi, S. Urabe, Hong–Ou–Mandel interference of two phonons in trapped ions. *Nature* **527**, 74-77 (2015).
7. A. M. Kaufman *et al.*, Two-particle quantum interference in tunnel-coupled optical tweezers. *Science* **345**, 306 (2014).
8. R. Lopes *et al.*, Atomic Hong–Ou–Mandel experiment. *Nature* **520**, 66-68 (2015).
9. J. Li *et al.*, Hong-Ou-Mandel Interference between Two Deterministic Collective Excitations in an Atomic Ensemble. *Phys Rev Lett* **117**, 180501 (2016).
10. R. C. Liu, B. Odom, Y. Yamamoto, S. Tarucha, Quantum interference in electron collision. *Nature* **391**, 263-265 (1998).
11. J. Dubois *et al.*, Minimal-excitation states for electron quantum optics using levitons. *Nature* **502**, 659-663 (2013).
12. D. Giovannini *et al.*, Spatially structured photons that travel in free space slower than the speed of light. *Science* **347**, 857-860 (2015).
13. M. D'Angelo, M. V. Chekhova, Y. Shih, Two-Photon Diffraction and Quantum Lithography. *Phys Rev Lett* **87**, 013602 (2001).
14. E. Knill, R. Laflamme, G. J. Milburn, A scheme for efficient quantum computation with linear optics. *Nature* **409**, 46-52 (2001).
15. J. Wang *et al.*, Multidimensional quantum entanglement with large-scale integrated optics. *Science* **360**, 285-291 (2018).
16. H.-S. Zhong *et al.*, Quantum computational advantage using photons. *Science* **370**, 1460-1463 (2020).
17. S. Aaronson, A. Arkhipov, paper presented at the Proceedings of the forty-third annual ACM symposium on Theory of computing, San Jose, California, USA, 2011.
18. J. Hofmann *et al.*, Heralded Entanglement Between Widely Separated Atoms. *Science* **337**, 72-75 (2012).
19. B. Jing *et al.*, Entanglement of three quantum memories via interference of three single photons. *Nat. Photonics* **13**, 210-213 (2019).
20. D. N. Makarov, Fluctuations in the detection of the HOM effect. *Sci Rep-Uk* **10**, 20124 (2020).
21. S. M. Barnett, J. Jeffers, A. Gatti, R. Loudon, Quantum optics of lossy beam splitters. *Phys. Rev. A* **57**, 2134-2145 (1998).
22. B. Vest *et al.*, Anti-coalescence of bosons on a lossy beam splitter. *Science* **356**, 1373-1376 (2017).
23. M. Michler, K. Mattle, H. Weinfurter, A. Zeilinger, Interferometric Bell-state analysis. *Phys Rev A* **53**, R1209-R1212 (1996).
24. K. Mattle, H. Weinfurter, P. G. Kwiat, A. Zeilinger, Dense Coding in Experimental Quantum Communication. *Phys Rev Lett* **76**, 4656-4659 (1996).
25. L. Sansoni *et al.*, Two-Particle Bosonic-Fermionic Quantum Walk via Integrated Photonics. *Phys Rev Lett* **108**, 010502 (2012).
26. A. Crespi *et al.*, Anderson localization of entangled photons in an integrated quantum walk. *Nat. Photonics* **7**, 322-328 (2013).
27. I. Pitsios *et al.*, Photonic simulation of entanglement growth and engineering after a spin chain quench. *Nat. Commun.* **8**, 1569 (2017).
28. B. Ndagano, A. Forbes, Entanglement distillation by Hong-Ou-Mandel interference with orbital angular momentum states. *APL Photonics* **4**, 016103 (2019).
29. M. Oszmaniec, N. Dangniam, M. E. S. Morales, Z. Zimboras, Fermion Sampling: a robust quantum computational advantage scheme using fermionic linear optics and magic input states. *arXiv*, (2020).
30. J. Wang, F. Sciarrino, A. Laing, M. G. Thompson, Integrated photonic quantum technologies. *Nat. Photonics* **14**, 273-284 (2020).
31. Q. Li *et al.*, A non-unitary metasurface enables continuous control of quantum photon–photon interactions from bosonic to fermionic. *Nature Photonics*, (2021).
32. A. N. Vetlugin, Coherent perfect absorption of quantum light. *arXiv:2101.02372 [quant-ph]*, (2021).
33. M. B. Plenio, S. F. Huelga, Entangled Light from White Noise. *Phys Rev Lett* **88**, 197901 (2002).
34. H. Krauter *et al.*, Entanglement Generated by Dissipation and Steady State Entanglement of Two Macroscopic Objects. *Phys Rev Lett* **107**, 080503 (2011).
35. D. G. Baranov, A. Krasnok, T. Shegai, A. Alu, Y. D. Chong, Coherent perfect absorbers: linear control of light with light. *Nat Rev Mater* **2**, 17064 (2017).
36. Y. D. Chong, L. Ge, H. Cao, A. D. Stone, Coherent perfect absorbers: time-reversed lasers. *Phys. Rev. Lett.* **105**, 053901 (2010).

37. W. Wan *et al.*, Time-Reversed Lasing and Interferometric Control of Absorption. *Science* **331**, 889-892 (2011).
38. J. Jeffers, Interference and the lossless lossy beam splitter. *J. Mod. Opt.* **47**, 1819-1824 (2000).
39. S. Huang, G. S. Agarwal, Coherent perfect absorption of path entangled single photons. *Opt. Express* **22**, 20936-20947 (2014).
40. T. Roger *et al.*, Coherent perfect absorption in deeply subwavelength films in the single-photon regime. *Nat. Commun.* **6**, 7031 (2015).
41. T. Roger *et al.*, Coherent Absorption of N00N States. *Phys. Rev. Lett.* **117**, 023601 (2016).
42. C. Altuzarra *et al.*, Coherent Perfect Absorption in Metamaterials with Entangled Photons. *Acs Photonics* **4**, 2124-2128 (2017).
43. A. Ü. C. Hardal, M. Wubs, Quantum coherent absorption of squeezed light. *Optica* **6**, 181-189 (2019).
44. A. Lyons *et al.*, Coherent metamaterial absorption of two-photon states with 40% efficiency. *Phys. Rev. A* **99**, 011801 (2019).
45. A. N. Vetlugin *et al.*, Coherent perfect absorption of single photons in a fiber network. *Appl. Phys. Lett.* **115**, 191101 (2019).
46. S. Yanikgonul *et al.*, Phase stabilization of a coherent fiber network by single-photon counting. *Opt. Lett.* **45**, 2740-2743 (2020).
47. A. Zeilinger, H. J. Bernstein, M. A. Horne, Information Transfer with Two-state Two-particle Quantum Systems. *J Mod Optic* **41**, 2375-2384 (1994).
48. J. Brendel, W. Dultz, W. Martienssen, Geometric phases in two-photon interference experiments. *Phys. Rev. A* **52**, 2551-2556 (1995).
49. Z. Y. Ou, E. C. Gage, B. E. Magill, L. Mandel, Fourth-order interference technique for determining the coherence time of a light beam. *J. Opt. Soc. Am. B* **6**, 100-103 (1989).
50. K. Hammerer, A. S. Sørensen, E. S. Polzik, Quantum interface between light and atomic ensembles. *Rev. Mod. Phys.* **82**, 1041-1093 (2010).
51. A. N. Vetlugin, I. V. Sokolov, Multivariate quantum memory as controllable delayed multi-port beamsplitter. *EPL* **113**, 64005 (2016).
52. J. L. Everett *et al.*, Time-reversed and coherently enhanced memory: A single-mode quantum atom-optic memory without a cavity. *Phys. Rev. A* **98**, 063846 (2018).
53. A. S. Losev, T. Y. Golubeva, A. D. Manukhova, Y. M. Golubev, Two-photon bunching inside a quantum memory cell. *Phys Rev A* **102**, 042603 (2020).
54. D. G. Baranov, A. Krasnok, A. Alù, Coherent virtual absorption based on complex zero excitation for ideal light capturing. *Optica* **4**, 1457-1461 (2017).
55. S. Zanotto *et al.*, Perfect energy-feeding into strongly coupled systems and interferometric control of polariton absorption. *Nature Physics* **10**, 830-834 (2014).
56. D. Zhang, X.-Q. Luo, Y.-P. Wang, T.-F. Li, J. Q. You, Observation of the exceptional point in cavity magnon-polaritons. *Nat Commun* **8**, 1368 (2017).
57. W. Xiong, J. Chen, B. Fang, C.-H. Lam, J. Q. You, Coherent perfect absorption in a weakly coupled atom-cavity system. *Phys Rev A* **101**, 063822 (2020).
58. A. Müllers *et al.*, Coherent perfect absorption of nonlinear matter waves. *Science Advances* **4**, eaat6539 (2018).